Nuclear Engineering and Design 399 (2022) 112005

Contents lists available at ScienceDirect

Nuclear Engineering and Design

journal homepage: www.elsevier.com/locate/nucengdes

Turbulent heat flux modelling in forced convection flows using artificial neural networks

Matilde Fiore [a,b,*], Lilla Koloszar [a], Miguel Alfonso Mendez [a], Matthieu Duponcheel [b], Yann Bartosiewicz [b]

[a] Von Karman Institute for Fluid Dynamics, Sint-Genesius-Rode 1640, Belgium
[b] Institute of Mechanics, Materials and Civil Engineering (IMMC), Université catholique de Louvain (UCLouvain), Place du Levant 2, 1348 Louvain-la-Neuve, Belgium

ARTICLE INFO

Keywords:
Prandtl number
Heat flux
Turbulence modelling
ANN

ABSTRACT

Fluid dynamics of liquid metals plays a central role in new generation liquid metal cooled nuclear reactors, for which numerical investigations require the use of an appropriate thermal turbulence model for low Prandtl number fluids. Given the limitations of traditional modelling approaches and the increasing availability of high-fidelity data for this class of fluids, we propose a machine learning strategy for the modelling of the turbulent heat flux. A comprehensive algebraic mathematical structure is derived and physical constraints are imposed to ensure attractive properties promoting stability and realizability. The closure coefficients of the model are predicted by an Artificial Neural Network (ANN) which is trained with the available Direct Numerical Simulation (DNS) data at different Prandtl numbers. The validation shows that the ANN provides an accurate representation of the heat flux in a wide range of Prandtl numbers (Pr = 0.01–0.71) and compares well with other existing thermal closures. Nevertheless, simulations with different auxiliary models to compute the inputs of the ANN revealed a certain sensitivity of the data-driven formulation on the models used in combination with it. In particular, the ANN model strongly relies on the Reynolds stress anisotropy. Such a sensitivity limits the robustness of the model to the inaccuracies of the underline momentum field and the momentum turbulence model applied in combination with it.

1. Introduction

Liquid metal heat transfer governs many phenomena and engineering applications, including high-performance cooling systems in new generation nuclear reactors. For such systems, the thermal-hydraulics conditions establishing during normal operation and transients must be carefully analysed for economic and safety reasons.

Due to the high cost of the experiments and their practical complexities, Computational Fluid Dynamics (CFD) became an important and complementary practice to support the design and testing of liquid metal cooled nuclear reactors. The numerical simulation of the reactor thermal hydraulics is challenged by the complex geometries and the high Reynolds numbers involved, which exclude the use of high-fidelity approaches as Direct Numerical Simulation (DNS) and Large Eddy Simulation (LES) to simulate the turbulent flows. The Reynolds Average Navier–Stokes (RANS) simulation of the reactor is less computational expensive, albeit affected by significant modelling uncertainties, due to the coexistence of different flow regimes (Roelofs, 2018) (in the fuel subassemblies and the pool) and the conductive properties of heavy liquid metals, whose Prandtl number is much lower than unity. Low Prandtl number flows are characterized by different sizes of thermal and momentum coherent structures and the consequent breakup of the similarity hypothesis at the basis of the well known Reynolds' analogy (Geankoplis, 2003). The eddy diffusivity approach provides then an inaccurate modelling of the heat flux, as shown in a number of available works (Grötzbach, 2013; Arien et al., 2004) on this topic. In particular, the assumptions of standard gradient diffusion and constant turbulent Prandtl number[1] appear questionable for heavy liquid metals.

Based on this evidence, the assessment of more sophisticated models for the turbulent heat flux became a priority in the nuclear research

* Corresponding author.
E-mail addresses: matilde.fiore@vki.ac.be (M. Fiore), lilla.koloszar@vki.ac.be (L. Koloszar), mendez@vki.ac.be (M.A. Mendez), matthieu.duponcheel@uclouvain.be (M. Duponcheel), yann.bartosiewicz@uclouvain.be (Y. Bartosiewicz).

[1] Recommended values for the turbulent Prandtl numbers are 0.85 for near unity Prandtl numbers and around 2.0 for low Prandtl number fluids.

https://doi.org/10.1016/j.nucengdes.2022.112005
Received 24 June 2022; Received in revised form 6 September 2022; Accepted 1 October 2022
Available online 3 November 2022
0029-5493/© 2022 Elsevier B.V. All rights reserved.

community and was sponsored by several European collaborative projects, as THINS (Papukchiev et al., 2015). These advanced thermal closures consist of correlations for the turbulent Prandtl number (Kays, 1994), the introduction of transport equations for the thermal turbulent statistics to compute thermal length and time scales rather than mechanical ones (Manservisi and Menghini, 2014), and the development of anisotropic closures (Shams et al., 2019) which do not assume the alignment of the heat flux with the mean temperature gradient. Nowadays, the validation of such low Prandtl based closures is limited to simple flow configurations at relatively low Reynolds numbers, for which reference data are available. Hence, the current validation range is too narrow to expect that the developed model generalize well for complex flow conditions and geometries. This explains why considerable efforts were put in other European projects as SESAME and MYRTE (Shams et al., 2020; Tarantino et al., 2020), to build an extensive low-Prandtl database for calibration and validation purposes.

Beside their use as reference to evaluate the existing models, these collected data represent an enormous source of information that should drive the construction of new models. The information should be extracted from data, summarized and translated in a mathematical form. In this regard, machine learning techniques are very useful to draw knowledge from big databases following structured methods. The use of these techniques in the context of turbulence modelling is continuously spreading. Current literature provides algebraic data-driven models to approximate the turbulent statistics (Ling et al., 2016b; Schmelzer et al., 2019) or data-driven corrections of their transport equations (Zhang and Duraisamy, 2015; Tracey et al., 2015; Singh et al., 2017). Among the available regression techniques, Artificial Neural Networks (ANNs) are often preferred to detect complex non-linear relationships and to efficiently handle very big datasets.

Compared to traditional approaches, the data-driven approach relies on data and, as such, it opens enormous challenges related to the generalization and the practical applicability of the developed formulation. If not properly trained and regularized, data-driven models can lead to unexpected or unphysical results when applied far from the conditions involved in the training. The model robustness needs to be increased by embedding essential physical and mathematical properties indirectly or by construction. Examples of essential properties are the invariance under rotation of the coordinate system (Ling et al., 2016a; Yin et al., 2020), the realizability of the Reynolds stresses (Jiang et al., 2021; Duraisamy et al., 2019), or the consistency with the second law of thermodynamics. Moreover, the predicted fields must have smooth derivatives, especially in the vicinity of the walls, to ensure the stable integration of RANS transport equations. In addition, thermal turbulence is a result of momentum turbulence and, consequently, a thermal turbulence model strongly relies on its momentum counterpart. This is the reason why advances in heat flux modelling are sought by simultaneously acting on both the type of closures in some research works (Abe et al., 1994, 1995). More generally, a non-isothermal turbulence simulation contains many models for thermal and momentum turbulence statistics which are mutually dependent. The coupling of the data-driven model with all the models involved in the numerical setup should be considered as well, to develop a robust formulation that does not amplify the uncertainties introduced by the associated submodels.

In this work, we present a deep-learning approach for the modelling of the turbulent heat flux that embeds essential physical and mathematical properties and aims at being valid in a wide range of Prandtl numbers and flow configurations. Herein, the ANN training is carried out using high-fidelity statistical data only, in order to construct a constitutive relationship for the closure term that does not compensate for the errors introduced by the additional sub-models of a typical RANS setup. This *frozen* training strategy assumes perfect thermal and momentum input quantities that do not exactly correspond to their counterparts given by thermal and momentum sub-closures. Consequently, the validation of the model in the CFD solver is a critical step of this methodology, as it needs to verify the effect of the model coupling beside its individual accuracy and stability. On this regards, an extensive validation of the data-driven model is provided in this work and guided the discussion related to its applicability and possible future developments.

The paper is organized as follows. Section 2 presents the mathematical structure of the model, the details of the artificial neural network and its training and the database used to train the model. Section 2 also briefly introduces other thermal turbulence models for low Prandtl numbers used for comparison and the auxiliary thermal and momentum turbulence models that were coupled with the data-driven formulation for the validation. Section 3 outlines the results of the ANN training, the *a priori* and *a posteriori* validation and highlights the limitations of the current formulation. Finally, conclusions and outlooks are provided in the last section.

2. Materials and methods

The data-driven approach is based on the development of a general mathematical structure that is presented in Section 2.1. The closure coefficients a_i and ω_i of the algebraic expression are then modelled with an artificial neural network, whose structure is defined in Section 2.2. The regularization method and the correction to prevent instabilities in the regions of vanishing temperature gradients are described in Section 2.3.

2.1. Mathematical formulation

This section outlines the derivation of the mathematical structure of the model. Additional details can be found in Fiore et al. (2021, 2022). The algebraic model for the turbulent heat flux $\overline{\mathbf{u}\theta}$ is based on a generalized gradient hypothesis for which the heat flux is written as the product of a dispersion tensor $\mathbf{D}$ with the mean temperature gradient:

$$\overline{\mathbf{u}\theta} = -\mathbf{D}\nabla T, \qquad \mathbf{D} = f\left(\mathbf{b}, \mathbf{S}, \boldsymbol{\Omega}, \|\nabla T\|, k, \epsilon, k_\theta, \epsilon_\theta, \alpha, \nu\right). \tag{1}$$

where the matrix notation is here adopted for tensors and $\mathbf{b}$, $\mathbf{S}$ and $\boldsymbol{\Omega}$ are given by

$$b_{ij} = \frac{\overline{u_i u_j}}{k} - \frac{2}{3}\delta_{ij}, \qquad S_{ij} = \frac{1}{2}\left(\frac{\partial U_i}{\partial x_j} + \frac{\partial U_j}{\partial x_i}\right),$$
$$\Omega_{ij} = \frac{1}{2}\left(\frac{\partial U_i}{\partial x_j} - \frac{\partial U_j}{\partial x_i}\right). \tag{2}$$

In Eqs. (1) and (2), U and u indicate the mean and fluctuating velocities, T and θ the mean and fluctuating temperature. The quantities k and k_θ denote the turbulent kinetic energy and the thermal variance, while ϵ and ϵ_θ the mechanical and thermal dissipation rates, respectively. The parameter ν is the kinematic viscosity, α is the thermal diffusivity. Eq. (1) implicitly assumes locality and instantaneity as a direct consequence of the algebraic structure. From a numerical point of view, this assumption is convenient, as it avoids the costs of a second order closure model for the heat flux. On the other hand, if transport equations are solved for k_θ and ϵ_θ, historical and non-local effects can be still implicitly represented, though at an isotropic level. Equilibrium turbulence is also assumed, since the gradients of the turbulent statistics (k, k_θ and b_{ij}) are not involved in the parametrization. This requires that the thermal turbulence production, destruction and redistribution mechanisms are more significant than transport ones, as it is assumed in many other works (So et al., 2004; So and Sommer, 1996; Wikström et al., 2000; Lazeroms et al., 2013) on this topic.[2]

[2] Clearly, this assumption is not satisfied in the near wall region, and requires the algebraic model to artificially mimic transport effects through the other parameters involved in the parametrization.

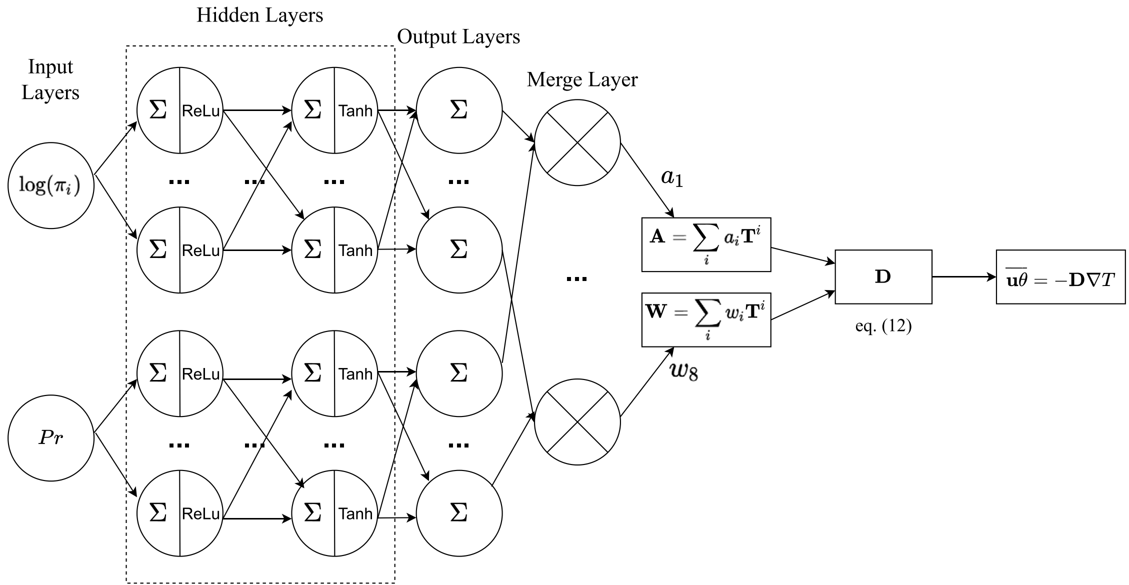

Fig. 1. Structure of the artificial neural network used to predict the turbulent heat flux as a function of the molecular Prandtl number and the basis of invariants indicated in Table 1.

The modelling of tensor **D** is aided by the introduction of physical and mathematical constraints that are convenient to get a general and realizable formulation. In particular, we seek to construct a model which satisfies invariance under rotation and which is consistent with the second law of thermodynamics.

The property of invariance under rotation requires to restrict the functional tensorial form indicated in Eq. (1) to all the possible linear mappings from **D** to a finite basis of independent tensors that can be formed from polynomials of tensors **b**, **S** and **Ω**. In practice, this constraint restricts the parameters of the non-linear regression problem to isotropic variables, i.e. quantities that are invariant under any rotation of the coordinate system. The consistency with the second law of thermodynamics requires that the real part of the eigenvalues of **D** are positive, to prevent conditions of reverse heat flux.

The above conditions were integrated into the model structure by applying the tensor representation theory (Spencer and Rivlin, 1997) under the assumption of statistically two-dimensional flows. This assumption reduces the tensors **S** and **Ω** to two-dimensional matrices and the tensor **b** to have zero off-diagonal components in the planes orthogonal to the plane of the flow. Accordingly, the basis of independent tensors and invariants indicated in Table 1, for the given set of parameters (Eq. (1)), is restricted compared to the more general, three-dimensional case. The Buckingham theorem was then applied to the set of independent scalar variables, here denoted as invariants. These steps led to the following definition of **D**:

$$\mathbf{D} = \left[(\mathbf{A} + \mathbf{A}^T)(\mathbf{A}^T + \mathbf{A}) + \frac{k}{\epsilon^{0.5}}(\mathbf{W} - \mathbf{W}^T) \right], \tag{3}$$

where **A** and **W** are written as linear combinations of the basis tensors $\mathbf{T}^i$ indicated in the second column of Table 1 :

$$\mathbf{A} = \sum_{i=1}^{n} a_i \mathbf{T}^i, \qquad \mathbf{W} = \sum_{i=1}^{n} w_i \mathbf{T}^i, \tag{4}$$

and a_i and w_i are arbitrary functions of the invariant dimensionless groups in first column of Table 1:

$$a_i = f_i(\pi_i, Re_t, Pr), \qquad w_i = g_i(\pi_i, Re_t, Pr). \tag{5}$$

Note that the tensors constituting the basis have dimensions of $\mathrm{m/s}^{1/2}$ to obtain a tensor of dimensions m^2/s after applying Eq. (3). This mathematical structure ensures that the model satisfies rotational invariance and realizability by construction, regardless of the particular functional form assumed for the coefficients a_i and w_i.

Table 1
Basis tensors and invariants.

Invariant basis	Tensor basis
$\pi_1 = \frac{k^2}{\epsilon^2}\{\mathbf{S}^2\}$, $\pi_2 = \frac{k^2}{\epsilon^2}\{\mathbf{\Omega}^2\}$, $\pi_3 = \frac{1}{\{\mathbf{b}\}}$,	$\mathbf{T_1} = \frac{k}{\epsilon^{1/2}}\mathbf{I}$, $\mathbf{T_2} = \frac{k}{\epsilon^{1/2}}\mathbf{b}$, $\mathbf{T_3} = \frac{k^2}{\epsilon^{3/2}}\mathbf{S}$,
$\pi_4 = \frac{k}{\epsilon}\{\mathbf{bS}\}$, $\pi_5 = \{\mathbf{b}_2\}$, $\pi_6 = \{\mathbf{bS\Omega}\}$,	$\mathbf{T_4} = \frac{k^2}{\epsilon^{3/2}}\mathbf{\Omega}$, $\mathbf{T_5} = \frac{k^2}{\epsilon^{3/2}}\mathbf{bS}$, $\mathbf{T_6} = \frac{k^2}{\epsilon^{3/2}}\mathbf{b\Omega}$,
$\pi_7 = \frac{\lvert\lvert\nabla T\rvert\rvert}{\sqrt{k_\theta}}\frac{k^{3/2}}{\epsilon}$, $\pi_8 = \frac{k_\theta \epsilon}{k\epsilon_\theta}$, $Re_t = \frac{k^2}{\epsilon\nu}$, $Pr = \frac{\nu}{\alpha}$	$\mathbf{T_7} = \frac{k^3}{\epsilon^{5/2}}\mathbf{S\Omega}$, $\mathbf{T_8} = \frac{k^3}{\epsilon^{5/2}}\mathbf{bS\Omega}$

2.2. Architecture of the neural network and training

The coefficients a_i and w_i of the expansion series introduced by Eq. (4) are modelled by an artificial neural network developed in the Pytorch[3] environment. The architecture of the ANN is depicted in Fig. 1: the network consists of two input layers for the invariant basis and the molecular Prandtl number, respectively. This choice is due to the analysis of the current parameter space, in which the molecular Prandtl number is the parameter explaining most of the heat flux variability. For the same flow configuration and Reynolds number, the change of the Prandtl number leads to significant variations of the heat flux distribution, while all the momentum statistics remain unchanged. The two separate branches help the network to find a good local minimum at the beginning of the training by rapidly optimizing the parameters of the second branch. For the rest of the training, the model is refined by optimizing the weights of the first branch. As shown in Fig. 1, the invariants undergo a logarithmic transformation $\hat{\pi}_i = \log(|\pi_i| + 1.0)$ before being injected in the input layer, since these scalar quantities are characterized by very high peaks in the near wall region that make the data distribution strongly right-skewed. The inputs are also re-scaled to fall the in the range $[-1, 1]$.

Six and one hidden layers are set for the first and the second branches of the network, respectively. The layers have 100 units each with rectified linear unit and hyperbolic tangent activation functions. The two branches of the network merge through a multiplication of the outputs performed in the final layer. Then, the turbulent heat flux is calculated following Eqs. (4) and (3). The cost function used for the training measured the error in the predicted heat flux and its first

[3] See https://pytorch.org/.

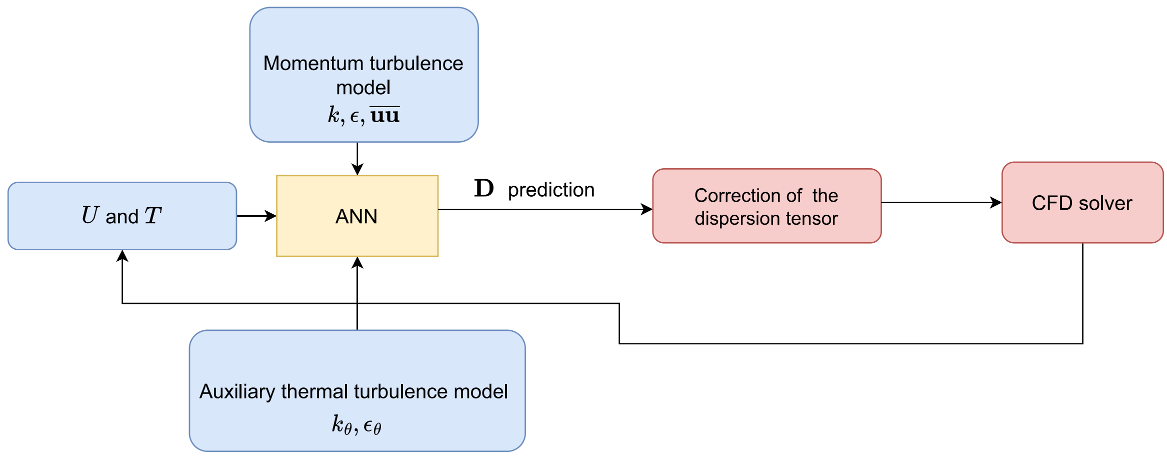

Fig. 2. Scheme of the model operation in the OpenFoam environment, with emphasis on the input quantities passed by the CFD solver and by the auxiliary momentum and thermal turbulence models.

spatial derivatives (Fiore et al., 2022) with respect to the values given by the DNS data:

$$\mathcal{L} = \frac{1}{N}\left(\sum_{i=1}^{N}\sum_{j=1}^{3}\left(\hat{q}_{i,j} - q_{i,j}\right)^2\right) + \frac{\lambda}{N}\left(\sum_{i=1}^{N}\sum_{j,k=1}^{3}\left|\frac{\partial \hat{q}_{i,j}}{\partial x_k} - \frac{\partial q_{i,j}}{\partial x_k}\right|\Delta x_k\right), \quad (6)$$

where $i \in [1, \dots N]$ is the index spanning across the N data points contained in each mini-batch, $q_{i,j} = \overline{u_j\theta}$ is the prediction of the ANN and $\hat{q}_{i,j}$ is the corresponding flux provided by DNS data. Both values $q_{i,j}$ and $\hat{q}_{i,j}$ are normalized with respect to the maximum DNS value achieved in each flow configuration. This cost function was preferred to the classical mean squared error to promote the smoothness of the predicted heat flux field. Smooth derivatives are essential for a good modelling, as the heat flux enters the energy equation through its divergence.

The network was trained using the Adaptive Moment Estimation (Adam) optimizer with a learning rate set to 0.001. The uncertainty of the heat flux predictions was estimated by applying the SWAG approach presented in Maddox et al. (2019) and Fiore et al. (2022). The approach assumes that the model uncertainty is correlated with the trajectory followed by the optimizer in the weight space. A multivariate Gaussian distribution is assumed for the network weights and this distribution is constructed through the weight averaging during the training. After the training, the uncertainty distribution of the output is estimated by sampling from the resulting weight posterior distribution and averaging the obtained predictions.

2.3. Noise addition and corrections

The algebraic structure of the model (Eq. (1)) is gradient driven by definition, i.e. it looses its theoretical justification where the heat flux does not correlate with the temperature gradient.[4] This means that the regression problem is ill-posed in some vanishing gradient regions where DNS simulations give finite values of the turbulent heat flux. One example is the region close to the centerline in case of non-isothermal turbulent channel flow: as shown in Fig. 3, the streamwise component of the heat flux reaches a non-zero value at the centerline, where the temperature gradient is zero. The ANN training would tend to compensate the flaws of this mathematical structure by increasing the magnitude of $\mathbf{D}$ in the vanishing gradient regions, to obtain a better fitting of the heat flux components. Two strategies were jointly applied during and after the training to mitigate this unphysical behaviour:

- **Noise addition**: during the training, $\|\nabla T\|$ is perturbed by adding noise from a Gaussian distribution of variance equal to 0.05% of the maximum temperature gradient in each flow configuration:

$$\widetilde{\|\nabla T\|} = \|\nabla T\| + \mathcal{N}(0, 5\cdot 10^{-4})\cdot \max_{x,y,z}\|\nabla T\| \quad (7)$$

  This approach is aimed at reducing the sensitivity of the network to the parameter π_7 (see Table 1), which is critical, since it could alter the natural linear dependency of $\overline{\mathbf{u}\theta}$ on its driving force ∇T.
- **Correction**: the symmetric part ($\mathbf{A}$) of the predicted dispersion tensor ($\mathbf{D}$) is a posteriori corrected to prevent extremely large values of $\mathbf{D}$:

$$\widetilde{A}_{i,j} = \begin{cases}\max\left(A_{ij}, 20\cdot\alpha_t\right), & \text{if } i = j\\ \min\left(\max\left(A_{ij}, -\sqrt{\prod_k A_{kk}}\right), \sqrt{\prod_k A_{kk}}\right), & \text{otherwise}\end{cases} \quad (8)$$

  where α_t is the turbulent thermal diffusivity calculated as specified by Manservisi and Menghini (2014). This correction is formally equivalent to limit the minimum value of the turbulent Prandtl number in presence of a standard gradient approach. Under the assumption of two-dimensional flow, this correction does not alter the conditions on the eigenvalues required to satisfy the second law of thermodynamics.

2.4. Description of the database

The database used to train the artificial neural network consists of DNS datasets related to different forced convection flows at various Re and Pr numbers. The details of the datasets are summarized in Table 2. Most of these databases concern standard, quasi two-dimensional flow configurations simulated at various Reynolds and Prandtl numbers and with different thermal boundary conditions. In particular, the databases of Kawamura et al. (2000), Tiselj et al. (2001), Bricteux et al. (2012) and Duponcheel et al. (2014) consist of DNS simulations of non-isothermal turbulent channel flow at Reynolds number ranging from $Re_\tau = 180$ to 2000 and Prandtl number from 0.01 to 0.71. Li et al. (2009) provided the DNS data of a non-isothermal turbulent boundary layer flow simulation at $Re_\theta = 800$, and Prandtl numbers of 0.71 and 0.2.

Beside these academic flows, additional three-dimensional flow configurations were used for training and test the current model to promote its robustness to real world applications. Specifically, the database of Oder et al. (2019) refers to a three-dimensional confined backward facing step flow at $Re_b = 3200$ and with an expansion ratio of 2.25. The forced convective heat transfer for this flow configuration was simulated at Prandtl numbers of 0.1 and 0.005, which is typical of

[4] This can happen during transients, in conditions of “return to isotropy” or in regions where the thermal turbulence is sustained by the intense turbulent transport.

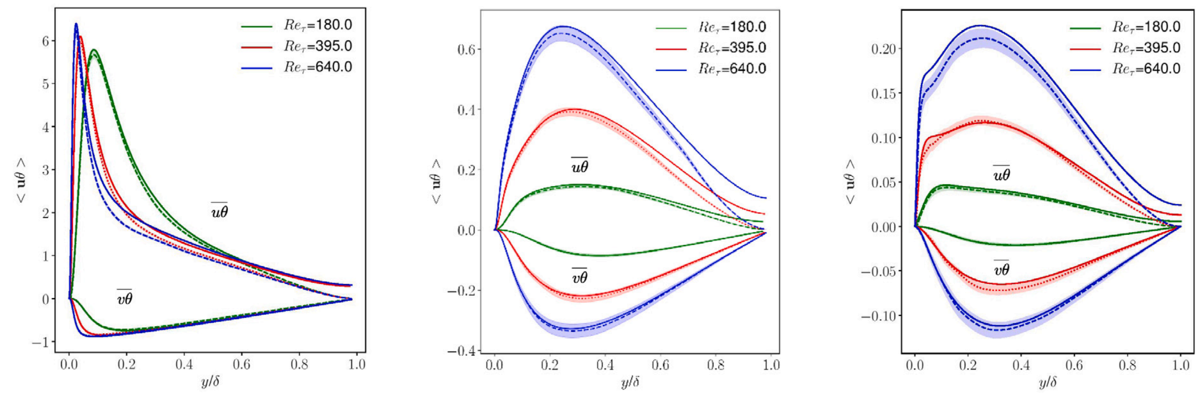

(a) $Pr = 0.71$ **(b)** $Pr = 0.025$ **(c)** $Pr = 0.01$

Fig. 3. Streamwise and wall-normal components of the turbulent heat flux predicted by the ANN after the training. Predictions in the training range and validation range are depicted with dashed and dotted lines, respectively. Shaded areas represent the uncertainty ranges of the heat flux predictions estimated with the SWAG algorithm (Maddox et al., 2019). DNS data (Kawamura et al., 2000) are indicated with solid lines.

sodium. Angeli et al. (2019) provided data related to convective heat transfer around cylindrical rods arranged in bundles. This kind of non-isothermal flow is of relevant interest in the nuclear reactor community, as it represents the cooling of reactor core fuel assemblies. This flow reaches a $Re_\tau = 550$ in the lattice subchannels and the $Pr = 0.031$ is considered as representative of liquid Lead–Bismuth Eutectic (LBE).

Table 2 also specifies the databases used for the training and the validation of the data-driven model. The Prandtl number of the training database ranged from a minimum value of 0.01 to the maximum of 0.71. The overall number of training points taken from the different databases amounts to 425 400 out of 500 000.

2.5. Some thermal turbulence models for low Prandtl numbers

As mentioned in Section 1, current literature provides other thermal turbulence models for low Prandtl number flows which are still under evaluation for complex geometries and/or flow conditions. These analytical models go beyond the Reynolds Analogy by adding terms to the constitutive relationship of the heat flux $\overline{u_i\theta}$, modifying the expression of the eddy diffusivity (e.g. introducing thermal or mixed time scales rather than dynamical ones) or by developing a transport model for the turbulent heat flux. An overview of some of these low-Prandtl based closures is given by Shams (2018). Some of these formulations have been used in the present work for the validation of the data-driven thermal model:

- The Manservisi and Meneghini model (Manservisi and Menghini, 2014) and the Kays correlation (Kays, 1994) are based on a standard gradient diffusion hypothesis:

$$\overline{u_i\theta} = -\alpha_t \frac{\partial T}{\partial x_i} \tag{9}$$

  the turbulent diffusivity α_t is modelled by Manservisi and Menghini (2014) as a function of k_θ and ϵ_θ, which are computed by solving two additional transport equations. This model was developed to be applied in combination with a $k-\epsilon$ type momentum turbulence model that is detailed in Ref. Manservisi and Menghini (2014). The Kays correlation (Kays, 1994) calculates α_t based on a variable turbulent Prandtl number, which is a function of Re_t and Pr.
- Shams et al. (2019) developed an algebraic model for $\overline{u_i\theta}$:

$$\overline{u_i\theta} = -C_{t0}\frac{k}{\epsilon}\left(C_{t1}\overline{u_iu_j}\frac{\partial T}{\partial x_j} + C_{t2}\overline{u_j\theta}\frac{\partial U_i}{\partial x_j} + C_{t3}\beta k_\theta g_i\right) + C_{t4}b_{ij}\overline{u_j\theta} \tag{10}$$

  where $\mathbf{g}$ is the gravity vector. The values of the closure coefficients $C_{t0} - C_{t4}$, as well as the transport equation for the thermal variance k_θ, can be found in Ref. Shams et al. (2019). Among the different AHFM formulations, this work considers the AHFM-EB that was calibrated to be applied in combination with the Elliptic Blending Reynolds Stress Model (EBRSM) implemented in the code Saturne.
- Dehoux et al. (2017) developed a Differential Transport Heat Flux Model (DTHFM) that is based on the elliptic blending concept for the modelling of the wall asymptotic behaviour:

$$\frac{\partial\overline{u_i\theta}}{\partial t} + U_j\frac{\partial\overline{u_i\theta}}{\partial x_j} = -\overline{u_iu_j}\frac{\partial T}{\partial x_j} - \overline{u_j\theta}\frac{\partial U_i}{\partial x_j} + D_{i\theta} + T_{i\theta} + \Phi_{i\theta} - \epsilon_{i\theta} \tag{11}$$

  for which the definition of the modelled molecular ($D_{i\theta}$) and turbulent ($T_{i\theta}$) transport terms, the redistribution term ($\Phi_{i\theta}$) and dissipation term ($\epsilon_{i\theta}$) are reported in Ref. Dehoux et al. (2017). The model was developed to be coupled with the EBRSM developed by Manceau (2015) and it has been validated for near unity Prandtl numbers in conditions of forced and mixed convection.

2.6. Auxiliary turbulence models employed for the validation

During the validation, the data-driven model is coupled with the momentum turbulence closures and other thermal submodels to compute its input turbulence statistics. The workflow is schematically depicted in Fig. 2, which indicates the variables directly passed by the CFD solver and the variables computed by the auxiliary thermal and momentum turbulence models. As regards the calculation of the Reynolds stresses, the choice of the model is critical due to the use of high fidelity data during the training. Two different momentum closures are combined with the data-driven model in the framework of this work:

- The EBRSM developed by Manceau (2005) which provides transport equations for the Reynolds stresses and employs the elliptic blending parameter to represent wall-blockage effects.
- The Launder–Sharma $k-\epsilon$ model, which relies on the Boussinesq assumption and the calculation of the eddy viscosity. As a consequence of the isotropy assumption, the anisotropic part of the Reynolds stress tensor $\mathbf{b}$ is roughly approximated by this model.

Regarding the estimation of k_θ and ϵ_θ needed to compute the invariants π_7 and π_8 indicated in Table 1, two different submodels are here used to support the ANN during the simulations:

- The Manservisi $k_\theta - \epsilon_\theta$ model briefly introduced in Section 2.5.

Table 2
Available DNS databases for forced convection at different Re and Pr numbers.

Author and Ref.	Flow configuration	Reynolds number[a]	Prandtl number	Usage
Kawamura et al. (2000)	Channel flow	Re_τ = 180–640	0.025–0.71	Training/test
Li et al. (2009)	Turbulent boundary layer	Re_θ = 830	0.2, 0.71	Training/test
Tiselj et al. (2001)	Channel flow	Re_τ = 180–590	0.01	Training/test
Oder et al. (2019)	Backward-facing step	Re_b = 3200	0.1,0.005	Training/test
Angeli et al. (2019)	Rode bundle flow	Re_τ = 550	0.031	Test
Bricteux et al. (2012) and Duponcheel et al. (2014)	Channel flow	Re_τ =180–2000	0.01–0.025	Test

[a]The complete definition of the Reynolds number for each flow configuration can be found in the related references.

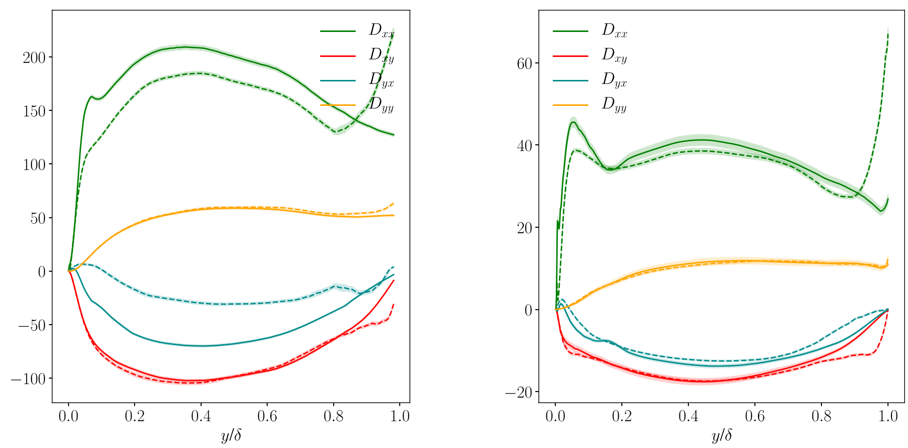

(a) $Pr = 0.71$ **(b)** $Pr = 0.025$

Fig. 4. Components of the dispersion tensor predicted by the ANN after the training for a non-isothermal channel flow at $Re_\tau = 395$. The solid lines indicate the results obtained by perturbing the parameter π_7. Dashed lines represent the results obtained without noise addition.

- The k_θ equation provided by Shams et al. (2019). This submodel does not provide a transport equation for the ϵ_θ, which is simply computed as $\epsilon_\theta = 2\frac{\epsilon k}{k_\theta}$.

3. Results and discussion

This section presents the results of the training and the validation of the data-driven model. The *a priori* validation consists in predicting the heat flux over high-fidelity (DNS) input data excluded from the training dataset. The *a posteriori* validation involves the integration of the model into the CFD code and the subsequent resolution of the transport equations using the data-driven thermal turbulence closure, together with conventional momentum turbulence models as the Launder–Sharma $k - \epsilon$ (Launder and Sharma, 1974) and the Elliptic Blending Reynolds stress model (Manceau, 2005).

3.1. A priori validation

Fig. 3 shows the results of the ANN training for cases of non-isothermal turbulent channel flow at different Prandtl numbers (Pr = 0.01 − 0.71). It is clear that the ANN is able to fit the DNS data in this wide range of Prandtl numbers, also matching the correct near wall behaviour for both the components of the turbulent heat flux. The accuracy of the predictions is similar for both training and test data, thus not showing problems of overfitting. Fig. 4 shows the components of the dispersion tensor obtained with the training for the same flow configuration, with and without noise addition. The noise addition leads to more reasonable distributions of the tensor components and mitigate the steep increase of **D** in the vanishing gradient regions.

The results of the training for the non-isothermal backward facing step flow are depicted in Fig. 5: also for this flow configuration, the network satisfactorily represents both the components of the turbulent heat flux along the step. The predicted field of the streamwise heat flux shows small inaccuracies close to the lower wall, where the data-driven model slightly overestimates the extension of the thermal separation region characterized by reverse heat flux. The lower accuracy detected in this region is probably due to the limitations of the algebraic mathematical structure, which is inherently local and makes hard to follow the abrupt evolution of the thermal field after the step.

The data-driven model was then used to predict the turbulent heat flux over the DNS data of the rode bundle flow (Angeli et al., 2019), which was not used for the model training. The turbulent heat flux predictions in the x and y directions are depicted in Figs. 6 and 7, where they are compared to the corresponding DNS data and the values obtained by applying the Kays correlation introduced in Section 2.5. The data driven model underestimates the peak values achieved by the heat flux in the gaps by around 10%, though its distribution agrees very well with the DNS counterpart and it is much better than the distribution given by the Kays correlation, which achieves the heat flux peaks very close to the bundle walls.

3.2. A posteriori validation

The *a posteriori* validation of the data driven model was carried out in OpenFoam 6.0.[5] The structure of the artificial neural network and its trained parameters were implemented into an existing library for thermal turbulence models. A similar implementation method is described in detail in the recent work of Maulik et al. (2021). The test cases selected for the *a posteriori* validation consist of non-isothermal channel flows at Re_τ up to 2000 and Pr numbers of 0.025 and 0.01, the backward facing step flow indicated in Table 2 at Prandtl number equal to 0.1 and 0.005 and the rod bundle flow simulated by Angeli et al. (2019) at Pr = 0.031.

[5] See https://www.openfoam.com/.

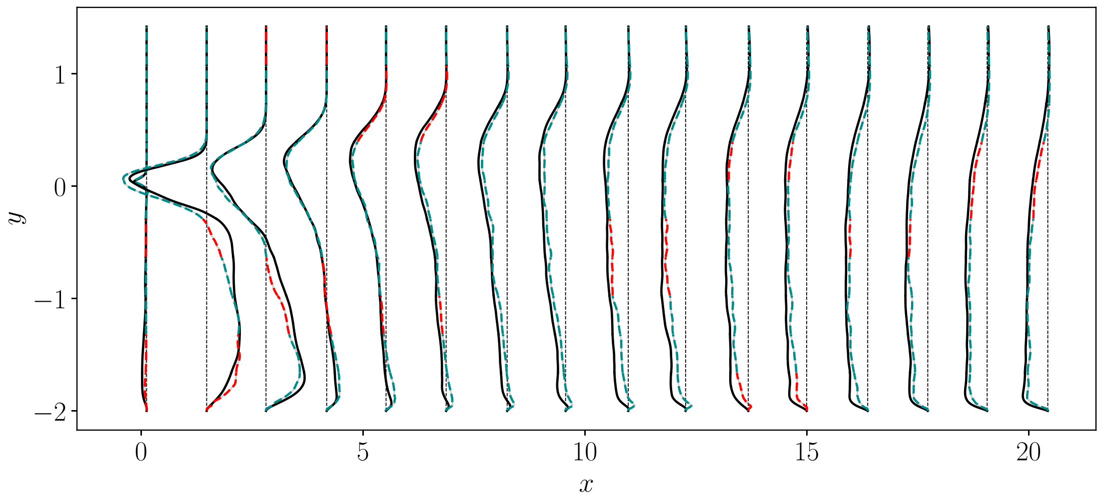

(a) Wall-normal heat flux

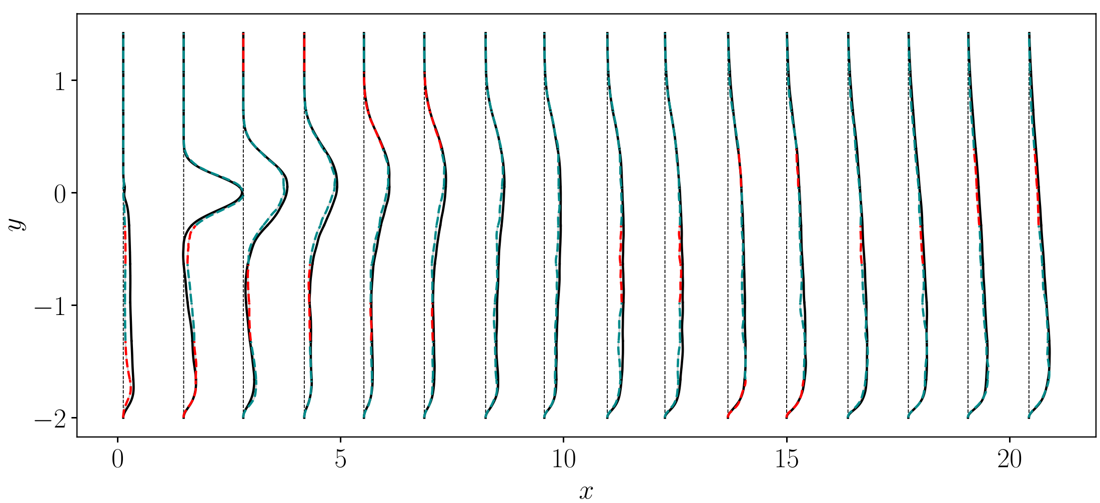

(b) Stream-wise heat flux

Fig. 5. Stream-wise and wall-normal components of the turbulent heat flux predicted by the ANN after the training for a non-isothermal, backward-facing step flow at $Pr = 0.1$. Predictions of training and validation data are depicted with blue and red dashed lines, respectively. DNS data (Oder et al., 2019) are represented with solid lines. (For interpretation of the references to colour in this figure legend, the reader is referred to the web version of this article.)

Non-isothermal turbulent channel flow

Fig. 8 shows the wall-normal turbulent heat flux predicted by the OpenFoam simulations carried out at different Reynolds and Prandtl numbers with the EBRSM as momentum turbulence model. For these simulations, the two-equations model developed by Manservisi and Menghini (2014) was used to compute k_θ and ϵ_θ. Even if the ANN was trained up to $Re_\tau = 640$ at $Pr = 0.025$ and up to $Re_\tau = 590$ at $Pr = 0.01$ (see Table 2), the model is able to extrapolate very well at higher Re_τ and accurately reproduces the correct heat fluxes at $Re_\tau = 2000$. These generalization properties are very important for the practical applicability of the formulation, as industrial problems usually involve much higher Reynolds numbers than those encountered in the current training database.

Figs. 9 and 10 (left) depicts the results of the channel flow simulations for $Re_\tau = 395$ and $Pr = 0.025$ and 0.01[6] and compare them with those obtained with the models presented in Section 2.5. The data-driven model proved to be very accurate for this kind of flow in terms of all the thermal statistics, except for the stream-wise component of the heat flux, which is more accurately predicted by the AHFM at $Pr = 0.01$. The predictions are more accurate than the models based on the standard gradient assumption (Manservisi and Menghini, 2014; Kays, 1994), as well as the anisotropic formulation developed by Shams et al. (2019). This confirms the potentialities of ANNs in the field of turbulence modelling, and shows that a wide exploration of the parameter space is useful to develop accurate and advanced thermal turbulence closures. Nevertheless, as mentioned in Section 2.5, each of this thermal models was developed to be applied in combination with a certain momentum turbulence model, which differs from the current EBM. Hence, another comparison of the models was carried out over a less accurate momentum field computed with the Launder–Sharma $k-\epsilon$ model. The results at $Pr = 0.025$ and $Re_\tau = 395$ are shown in Fig. 10 (right). The data driven model overestimates the wall-normal heat flux by almost 50%, being less robust than the other thermal models, which show the ability to better adapt to different momentum

[6] Note that these conditions were excluded from the training dataset (see Table 2) to ensure a meaningful validation.

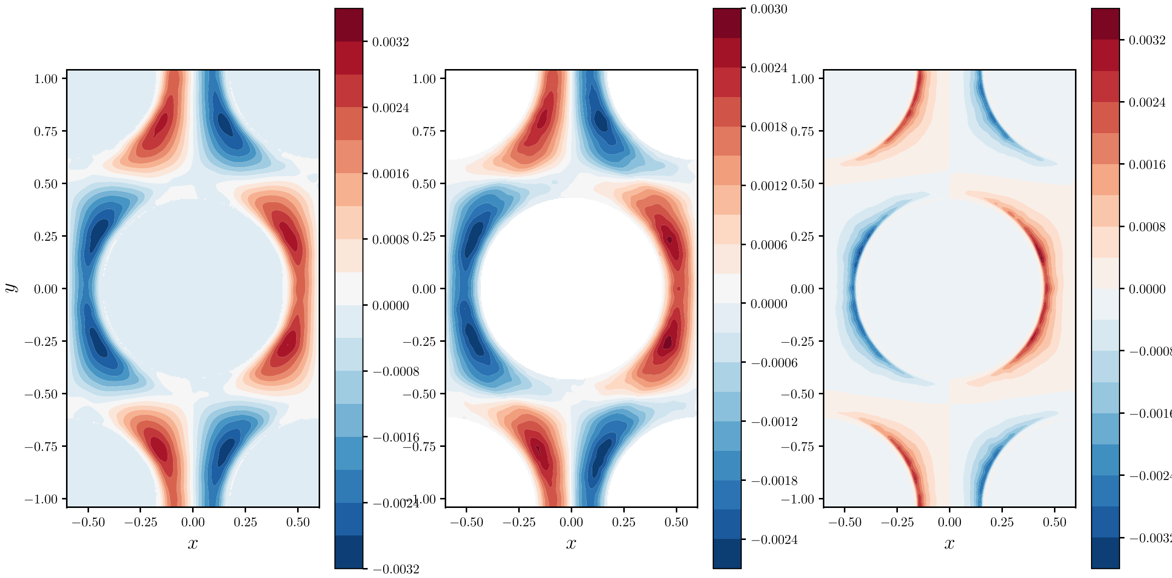

Fig. 6. Contours of the x-component of the turbulent heat flux for the rode bundle flow. Left to right: DNS data (Angeli et al., 2019), predictions of the data-driven model and predictions of the Kays correlation.

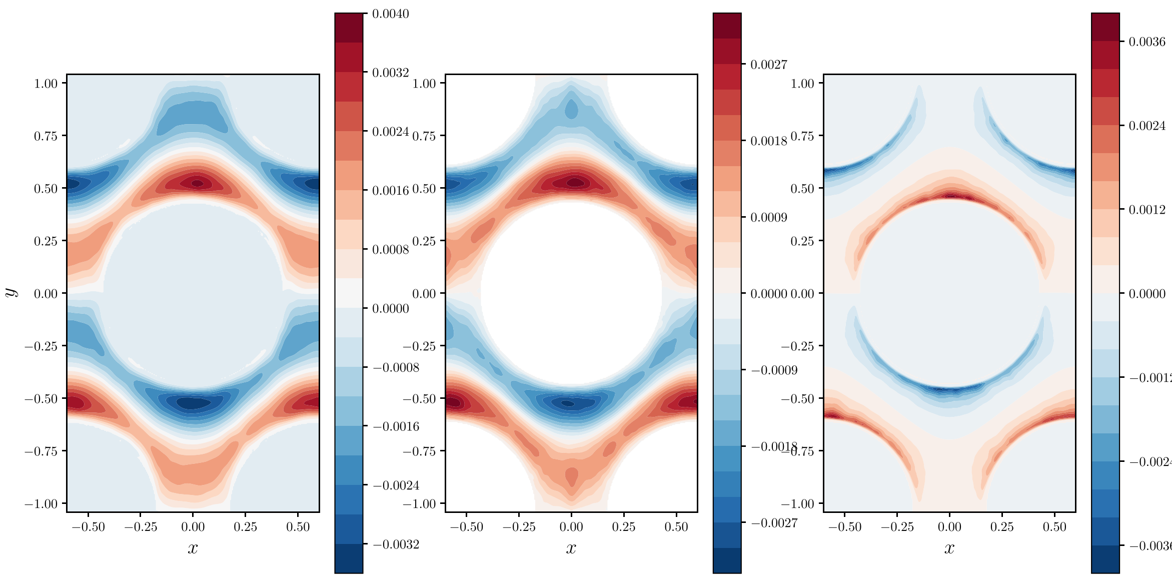

Fig. 7. Contours of the y-component of the turbulent heat flux for the rode bundle flow. Left to right: DNS data (Angeli et al., 2019), predictions of the data-driven model and predictions of the Kays correlation.

treatments. This lack of robustness is due to the anisotropic character of the data-driven formulation and its complexity, i.e. the wide range of parameters accounted (Table 1) which are not all accurately estimated by the auxiliary momentum turbulence model.

Non-isothermal backward-facing step flow

The second flow configuration considered for the validation is the backward facing step flow simulated by Oder et al. (2019) at $Pr = 0.1$ and $Pr = 0.005$. The original DNS simulation showed a secondary flow recirculation in the spanwise direction due to the presence of the lateral walls. However, in the mid-plane, the spanwise velocity components are practically zero and the flow can be considered locally two-dimensional. Based on this consideration, the thermal field on the mid-plane was simulated in OpenFoam by employing a two-dimensional geometry. The momentum field was not simulated, though it was directly mapped from the corresponding DNS data (Oder et al., 2019). For these simulations, the data-driven model was combined with the $k_\theta - \epsilon_\theta$ equations developed by Manservisi. The results in terms of temperature and heat flux are compared with the ones obtained by applying the Kays correlation (Kays, 1994) and the algebraic heat flux model (Shams et al., 2019) presented in Section 2.5.

Figs. 11, 12 and 13 show the contours of the temperature field and the turbulent heat flux components obtained by applying the data-driven model at the two values of the Prandtl numbers, and their comparison with the corresponding DNS distributions. Although the lowest value of Pr covered by the training was 0.01 and the network was only trained at $Pr = 0.1$ for this flow configuration, the heat flux predictions are in good agreement with the DNS data also at $Pr = 0.005$. The model is able to capture the change of sign of the streamwise heat flux in the separation region, as shown by Fig. 12(a). The extension of this zone of thermal separation and mixing is overestimated by the model at $Pr = 0.1$, as already seen in the a priori validation (see Fig. 5).

Figs. 14, 15 and 16 shows the heat flux at temperature profiles over the channel width at several distances from the step, as they results

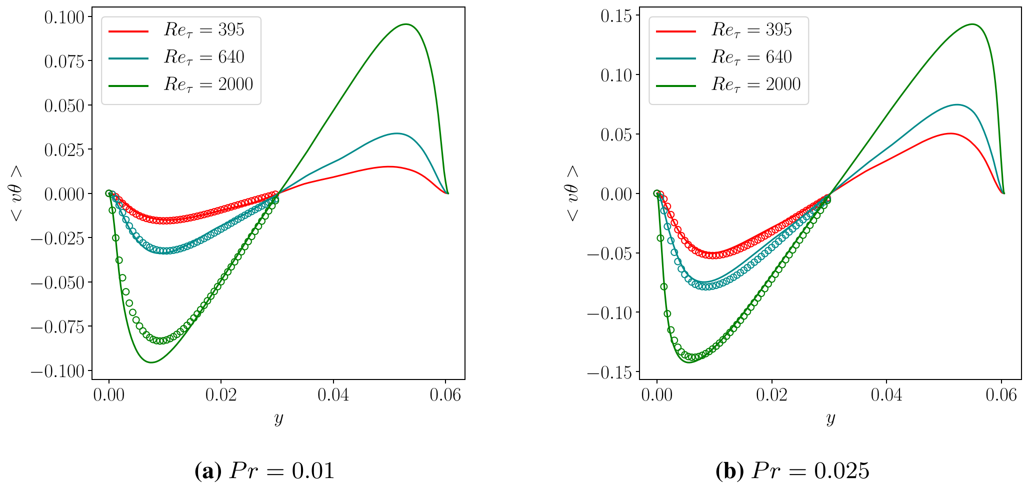

(a) $Pr = 0.01$ **(b)** $Pr = 0.025$

Fig. 8. Comparison of the wall-normal heat flux computed with the data-driven model with the corresponding DNS (Kawamura et al., 2000) and LES data (Duponcheel et al., 2014) for simulations of non-isothermal turbulent channel flows at Re_τ up to 2000.

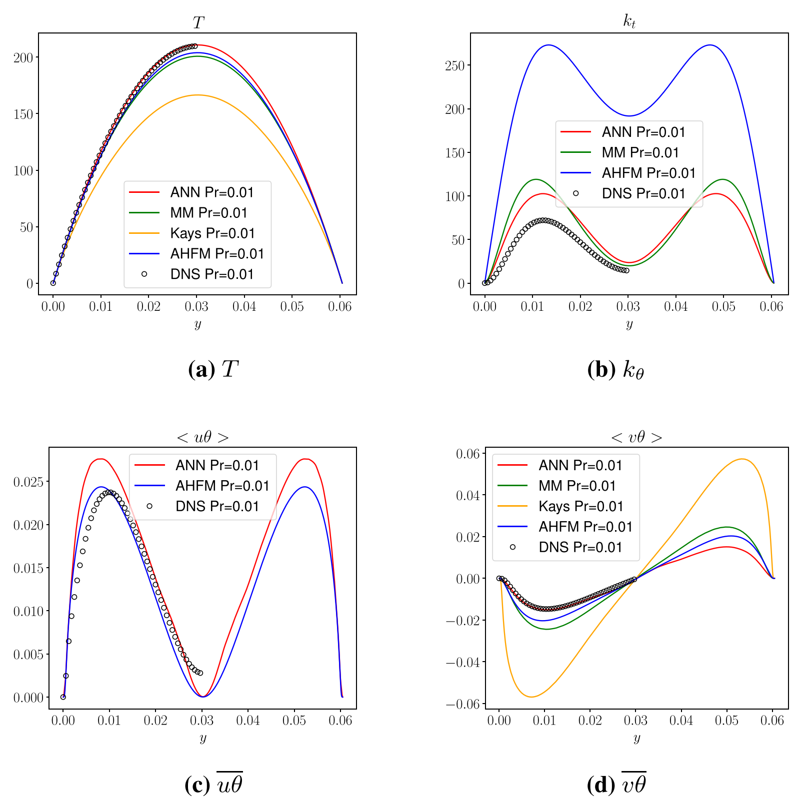

(a) T **(b)** k_θ

(c) $\overline{u\theta}$ **(d)** $\overline{v\theta}$

Fig. 9. Comparison of the results achieved with the data-driven model (ML), the Manservisi model (MM), the Kays correlation and the AHFM model at $Re_\tau = 395$ and $Pr = 0.01$.

from the application of the data-driven model, the Kays correlation and the AHFM. The ANN tends to overpredict the heat flux at $Pr = 0.1$, and the comparison with the DNS data is slightly worse than in the a priori validation (see Fig. 5). This means that the link with the other transport equations have a significant impact on the model performance for this particular flow. However, the near wall behaviour of the predicted heat flux is more accurate than for the other models. At $Pr = 0.005$, the heat flux values predicted by the ANN are closer to the DNS ones with respect to the ones given by the AHFM and the Kays correlation, which tend to underestimate its values.[7] However, above the stream region, the heat flux is under predicted by the data-driven model and this explains why, at a certain distance from the step, the temperature is

[7] Note that, at $Pr = 0.005$, the conductive flux is much higher than the turbulent flux at this Reynolds number. This explains why the temperature profiles obtained with the other models (Fig. 14(b)) at $Pr = 0.005$ are in substantial agreement with the DNS ones, although the turbulent heat flux is misrepresented.

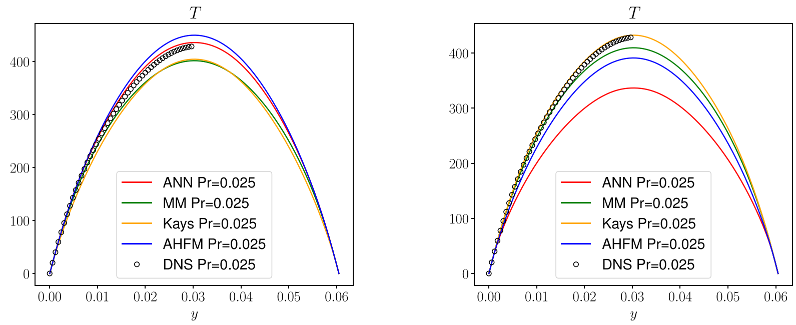

(a) T

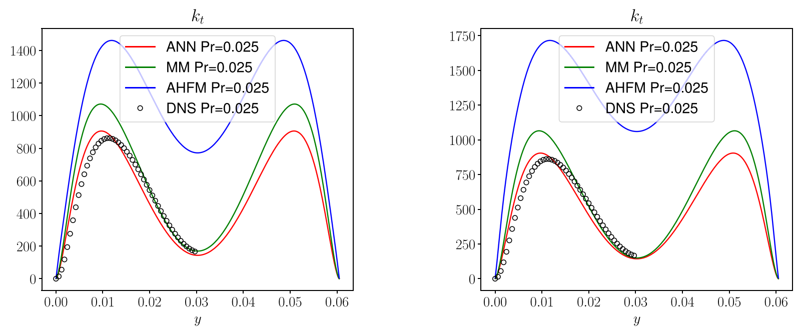

(b) k_θ

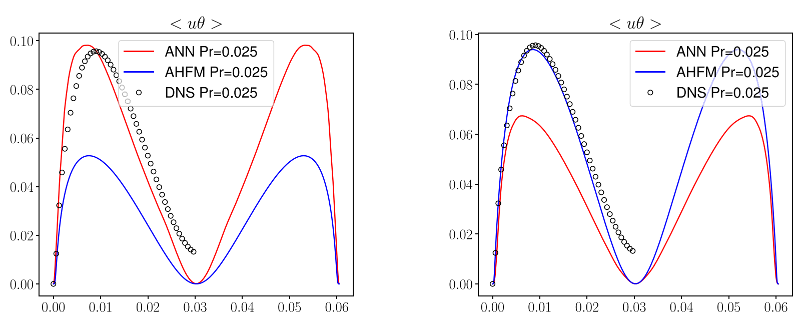

(c) $\overline{u\theta}$

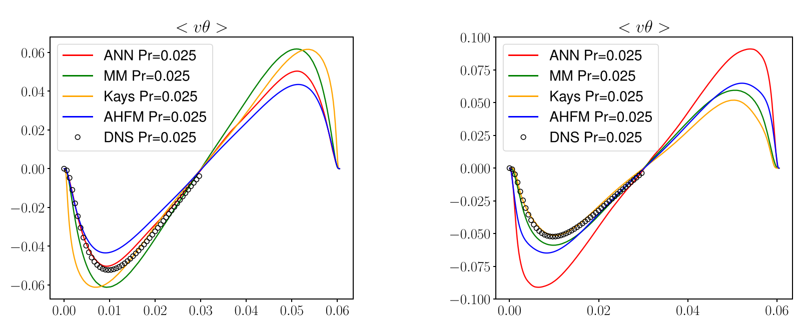

(d) $\overline{v\theta}$

Fig. 10. Comparison of the results achieved with the data-driven model (ML), the Manservisi model (MM), the Kays correlation and the AHFM model at Re_τ = 395 and Pr = 0.025 as thermal turbulence models, and the EBM (left) and the Launder–Sharma $k-\epsilon$ (right) as momentum turbulence models.

lower than the DNS one close to the upper wall of the channel. In the separation and reattachment region, the temperature profiles obtained with the data-driven model are more accurate than the ones given by the other thermal model at both the values of the Prandtl number.

Rod bundle flow

The last test case consists of a non-isothermal flow over vertical rods arranged in bundles, which is a typical benchmark in nuclear engineering to study the heat transfer through nuclear fuel assemblies.

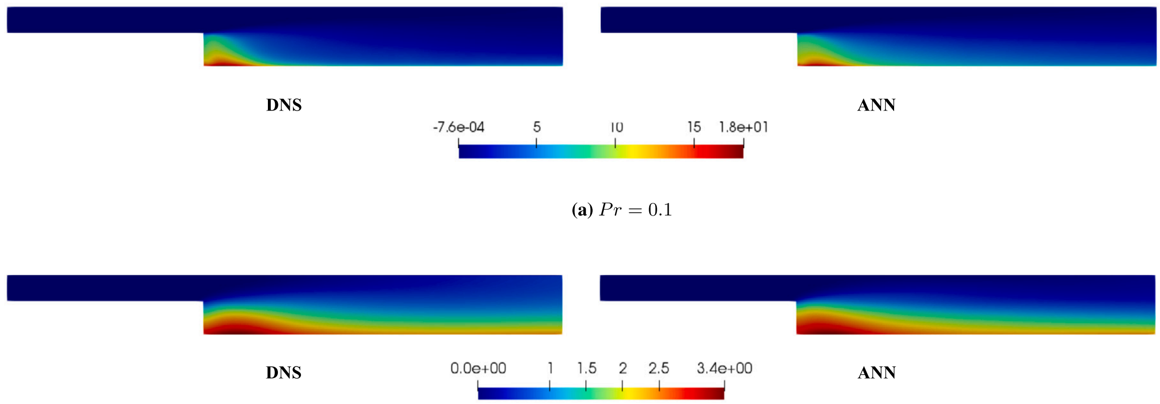

(a) $Pr = 0.1$

(b) $Pr = 0.005$

Fig. 11. Temperature distributions obtained with the data-driven thermal turbulence model (ANN). Comparison with the corresponding DNS data (Oder et al., 2019).

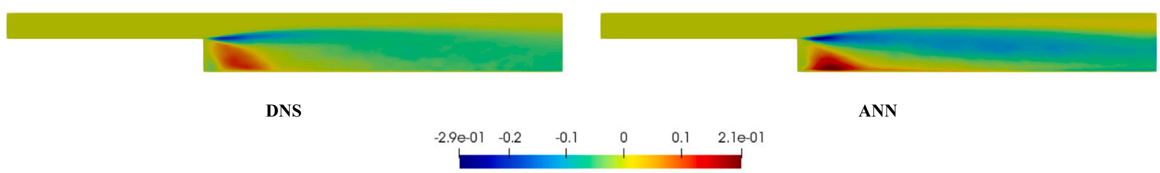

(a) $Pr = 0.1$

(b) $Pr = 0.005$

Fig. 12. Streamwise heat flux distributions obtained with the data-driven thermal turbulence model (ANN). Comparison with the corresponding DNS data (Oder et al., 2019).

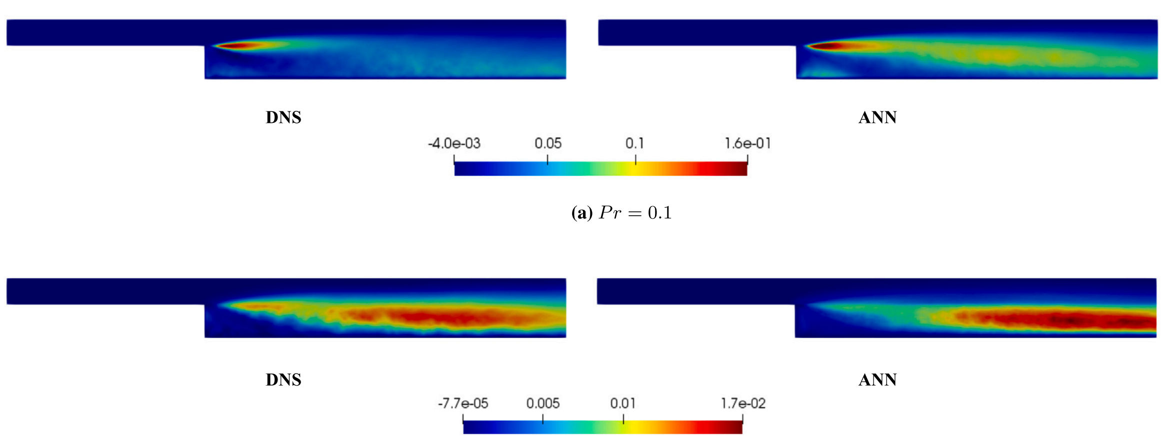

(a) $Pr = 0.1$

(b) $Pr = 0.005$

Fig. 13. Wall-normal heat flux distributions obtained with the data-driven thermal turbulence model (ANN). Comparison with the corresponding DNS data (Oder et al., 2019).

The numerical setup reproduces the same thermal and flow conditions investigated by Angeli et al. (2019) with the direct numerical simulation. This bundle arrangement is characterized by a pitch-to-diameter equal to 1.4. A rectangular cell consisting of 4 subchannels

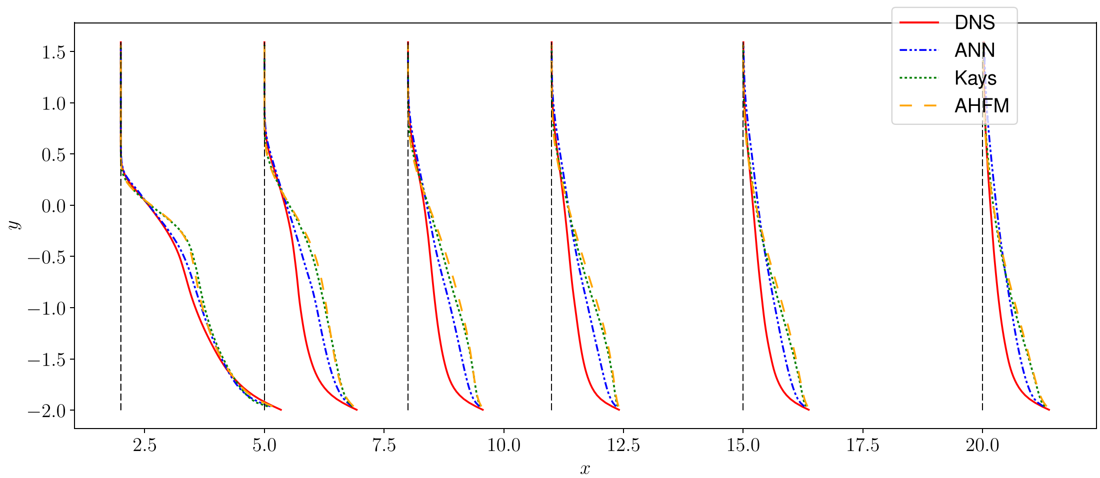

(a) $Pr = 0.1$

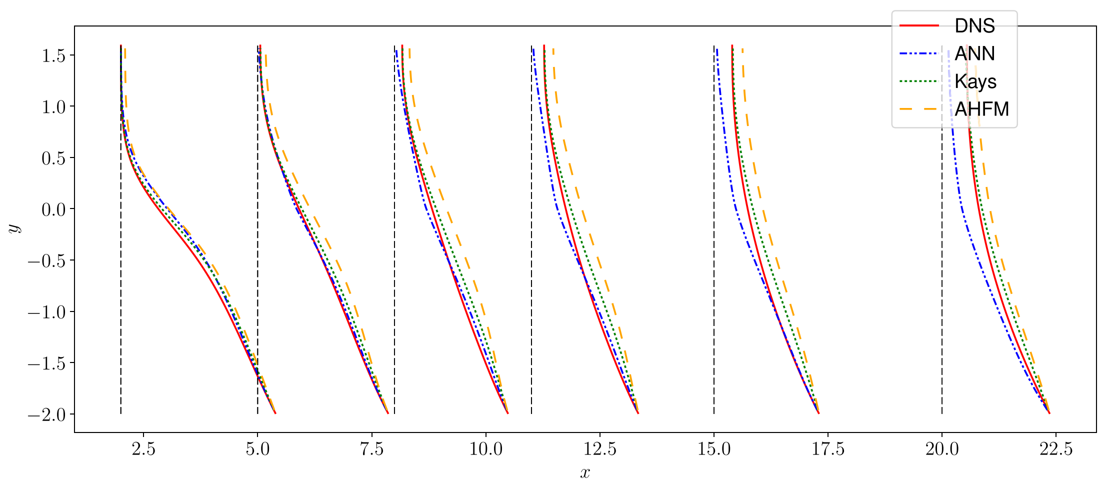

(b) $Pr = 0.005$

Fig. 14. Temperature profiles obtained at several distances from the step with the data-driven model (ANN), the Kays correlation (Kays, 1994) and the algebraic model developed by Shams et al. (2019) (AHFM). Comparison with the corresponding DNS data (Oder et al., 2019).

is constructed as schematized in Fig. 17. An unstructured hexahedral mesh of 584 000 cells was generated to simulate this flow. As shown in Fig. 18, the mesh is refined close to the cylindrical walls where layers were added to simulate the boundary layers. The first cells near the cylinder walls correspond to y^+ values ranging from 0.45 to 0.55, which allows to apply a wall resolved approach for both thermal and momentum turbulence.

Cyclic boundary conditions are applied at all the fluid boundaries in the x, y and z directions, and a condition of uniform heat flux is imposed at the cylinder walls. A mechanical source term is added to the momentum equations to reach a bulk Reynolds number of 8290. As explained in Ref. Angeli et al. (2019), a source term is added to the energy equation to account for the linear increase of the temperature in the streamwise direction (z axis):

$$S_\theta = -\frac{W}{W_b}\frac{P}{A}\dot{q_w} \tag{12}$$

where P indicates the perimeter of the rods, A is the area crossed by the flow, $\dot{q_w}$ is the heat flux imposed at the cylinder walls and W and W_b denote the local and bulk streamwise velocities, respectively.

Thanks to the absence of separation and recirculation zones for this flow configuration, the EBRSM achieved a convergent solution and its velocity profile along the flow cell is in better agreement with the DNS one than the one obtained with the $k-\epsilon$ and $k-\omega$ SST models, as indicated in Fig. 19(a). The agreement of the momentum statistics in represented in Fig. 19, where the distribution of the velocity and the Reynolds stresses are compared with the DNS data over the cylindrical coordinate γ, which corresponds to the conjunction of the largest and smallest paths connecting two rods (see Fig. 17).

Several thermal turbulence models are applied under these flow conditions. The data-driven model was combined both with the $k_\theta - \epsilon_\theta$ model of Manservisi (ANN:MM) and the k_θ equation of Shams (ANN:Shams). As mentioned in Section 3.1, this turbulent flow is fully three-dimensional and was not used as training dataset to develop the data-driven model. The comparison of the results in terms of thermal variance is indicated in Fig. 20(a). None of the models applied seems able to accurately represent the behaviour of k_θ: the Manservisi model and the data-driven closure coupled with the same transport equations for k_θ and ϵ_θ underestimate the correct thermal variance, while the other models based on different k_θ equations overestimate it. In particular, the AHFM developed by Shams shows to be the most accurate to represent this thermal statistics.

The profiles of the turbulent heat flux components over the same path are indicated in Figs. 20(b), 20(c) and 20(d). The results obtained with the different models significantly vary in terms of peak values

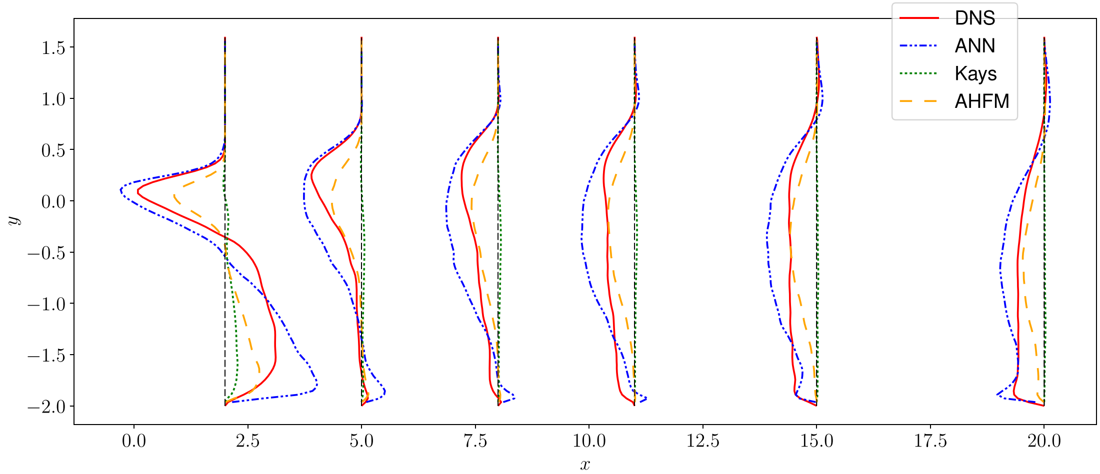

(a) $Pr = 0.1$

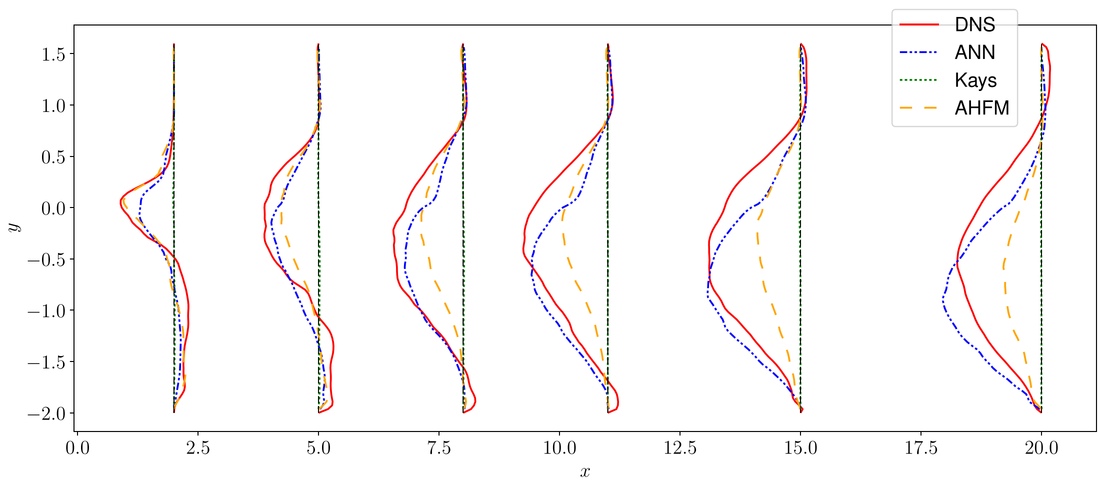

(b) $Pr = 0.005$

Fig. 15. Streamwise heat flux profiles obtained at several distances from the step with the data-driven model (ANN), the Kays correlation (Kays, 1994) and the algebraic model developed by Shams et al. (2019) (AHFM). Comparison with the corresponding DNS data (Oder et al., 2019).

Table 3
Values of the Nusselt number obtained by simulating the rod bundle flow with several thermal turbulence closures.

	DNS	Manservisi (Manservisi and Menghini, 2014)	AHFM:EB (Shams et al., 2019)	DTHFM (Dehoux et al., 2017)	ANN:MM	ANN:Shams
Nusselt number	12.82	11.54	12.35	11.13	12.04	12.84

and shape of the heat flux profiles. As regards the data-driven model, the heat flux distribution achieved at convergence is considerably affected by the auxiliary transport equation applied to compute k_θ. The temperature profiles obtained with the different thermal models are compared in Fig. 21. Most of the models applied tend to overpredict the ΔT developing between the core of the flow and the cylinder walls. This result is in agreement with the values of the Nusselt number reported in Table 3, which show that the convective heat flux is underpredicted by all the thermal models under consideration, except for the data-driven model coupled with k_θ equation of Shams, which predicts a very accurate value of the Nusselt number.

Based on the current results, the most accurate thermal treatments for this flow, when combined with the EBRSM for the Reynolds stresses, are the AHFM developed by Shams et al. (2019) and the current data-driven turbulence model.

The validation test cases presented in this section proved the applicability of the data-driven model to several flow configurations and its good comparison with other thermal closures. On the other hand, these simulations highlight the sensitivity of the data-driven model to the momentum closure and the thermal submodels applied in combination with it. Indeed, the model is trained on high-fidelity data of utmost accuracy. Such a level of accuracy is not always expectable in a RANS simulation, where many submodels contribute to propagate uncertainties to all the computed fields. The resulting inaccuracies in the momentum and thermal statistics can be significant, especially if the flow is characterized by complex structures. Hence, this high sensitivity to the auxiliary models poses limits to the reliability of the results obtained with the data-driven model when in its input turbulent statistics are affected by high uncertainties.

4. Conclusions

This work presents a data-driven approach for the modelling of the turbulent heat flux with special focus to low Prandtl number flows,

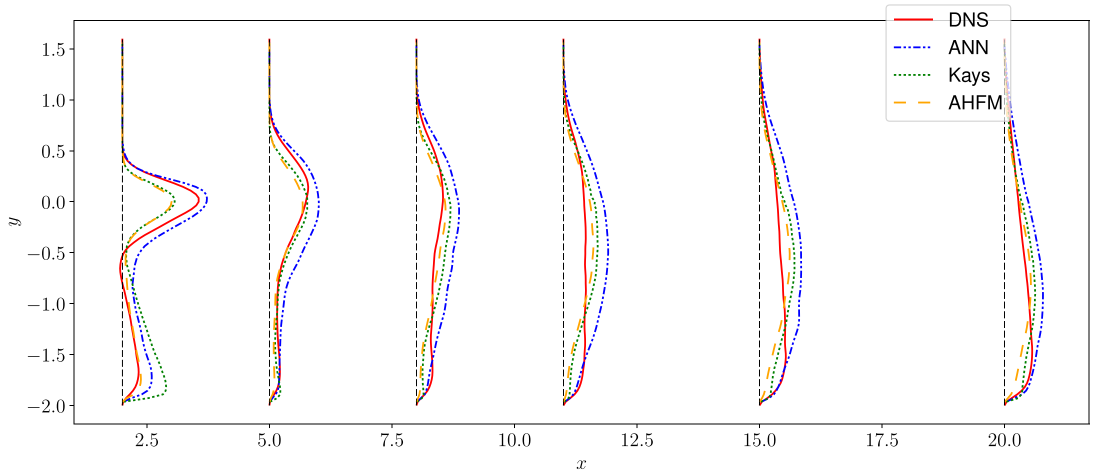

(a) $Pr = 0.1$

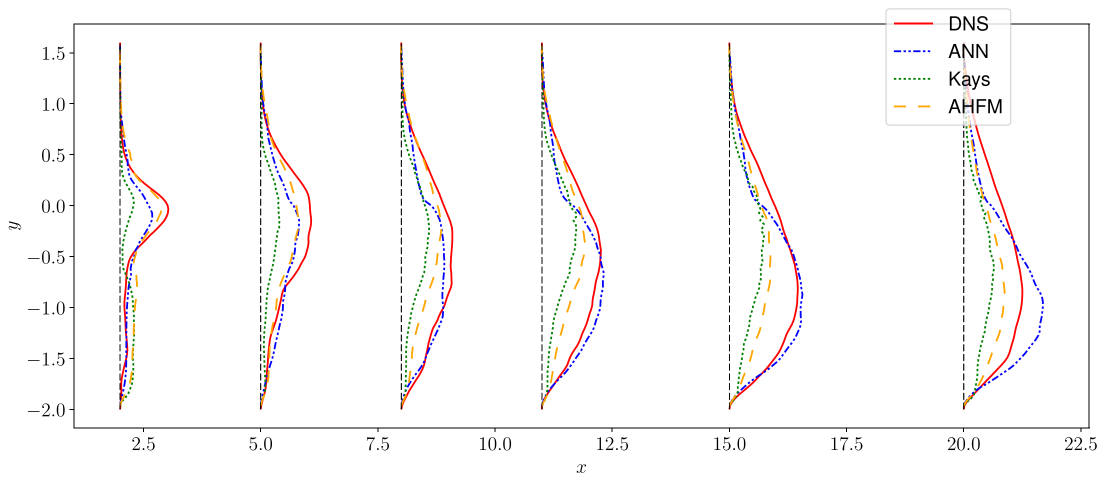

(b) $Pr = 0.005$

Fig. 16. Wall-normal heat flux profiles obtained at several distances from the step with the data-driven model (ANN), the Kays correlation (Kays, 1994) and the algebraic model developed by Shams et al. (2019) (AHFM). Comparison with the corresponding DNS data (Oder et al., 2019).

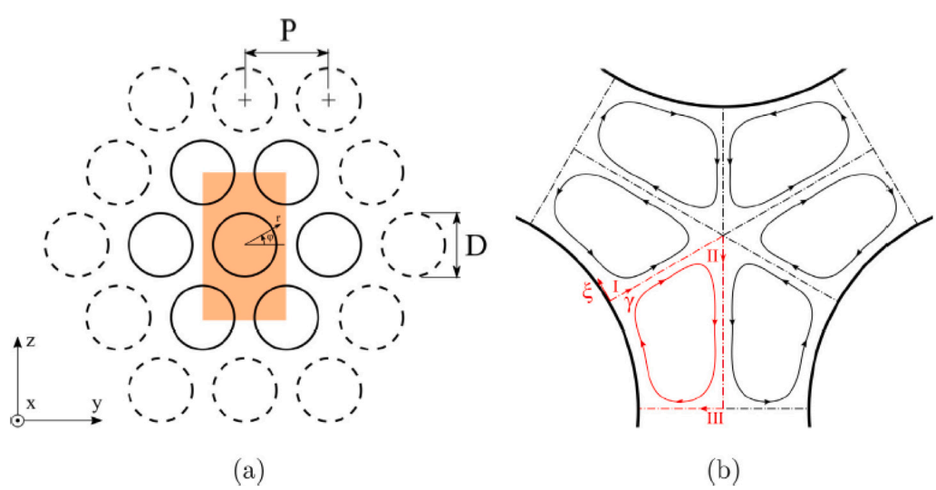

Fig. 17. Problem description: (a) schematic of the cross-section of the infinite triangular rod bundle. The module comprising four subchannel is highlighted; (b) schematic of a subchannel containing 6 unit flow cells ; the border of the unit flow cell (coloured in red) is subdivided into three segments I, II and III, and endowed with a local system of curvilinear tangential and normal coordinates. (For interpretation of the references to colour in this figure legend, the reader is referred to the web version of this article.)

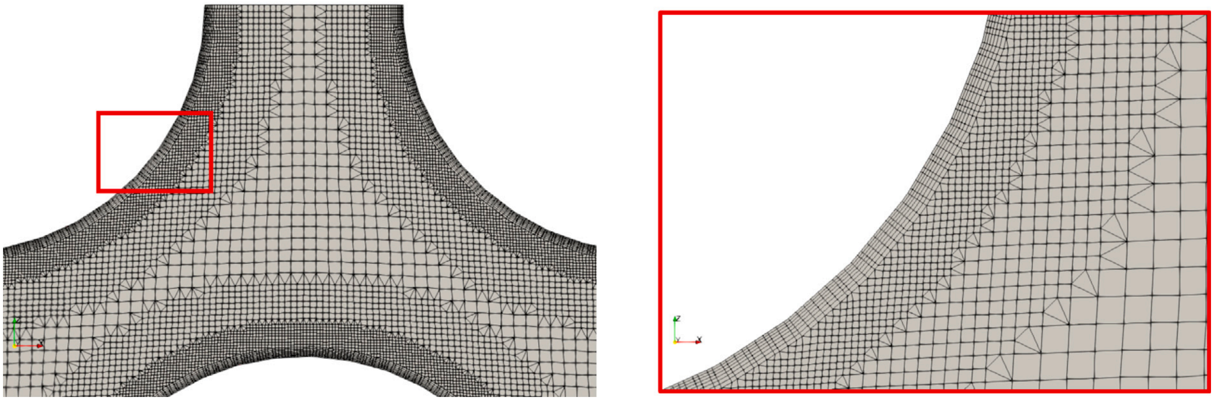

Fig. 18. Cross-section view of the mesh used for the simulation of the rod bundle flow. On the right, the picture is zoomed in to show the layers surrounding the cylinder walls.

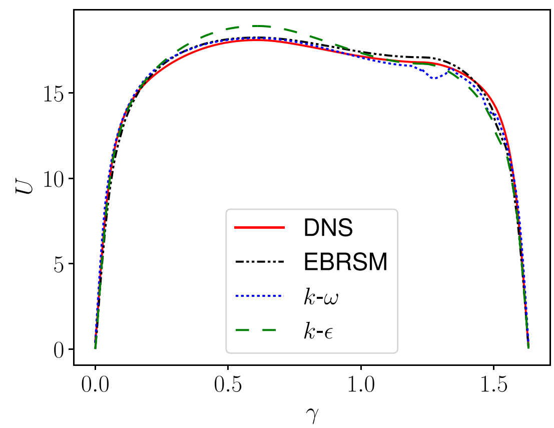

(a) Mean velocity

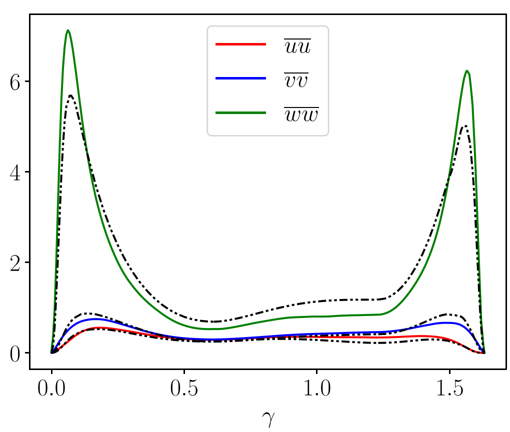

(b) Diagonal stresses

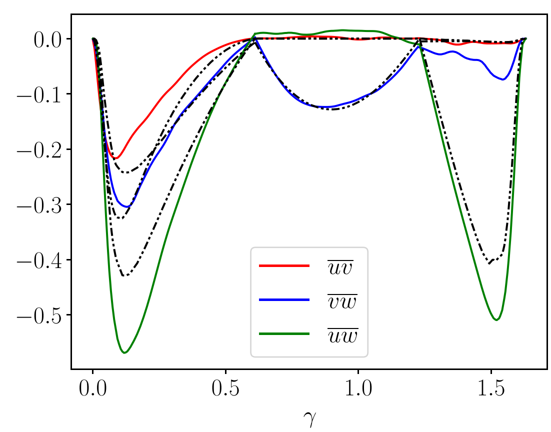

(c) Off-diagonal stresses

Fig. 19. Distributions of the momentum statistics along the border of the flow cell depicted in Fig. 17. Top: streamwise velocity computed with several momentum turbulence models. Bottom: components of the Reynolds stress tensor.

which are currently under investigation in view of new generation liquid metal cooled nuclear reactors. The algebraic structure of the model embeds invariance and realizability properties, and the training methodology ensured smooth predictions and good generalization. The training database covered a wide range of Prandtl numbers ($Pr = 0.01-0.71$) and flow configurations to achieve a general and unified formulation. A correction is applied on the tensor a posteriori to prevent its unphysical behaviour in regions where the temperature gradient is vanishing. The correction does not alter the realizable and rotationally invariant characters of the model.

The *a priori* and *a posteriori* validation concerned different two-dimensional and three-dimensional flow configurations in the low Prandtl number regime. The results showed that the data-driven model has great interpolation and extrapolation properties and adapts for Reynolds numbers, Prandtl numbers and flow configurations not covered by the current training database. When applied in combination with a wall-resolved, second order momentum turbulence model and then compared to other thermal models for low Prandtl numbers, the model showed to be very accurate and satisfactorily reproduced the different components of the turbulent heat flux.

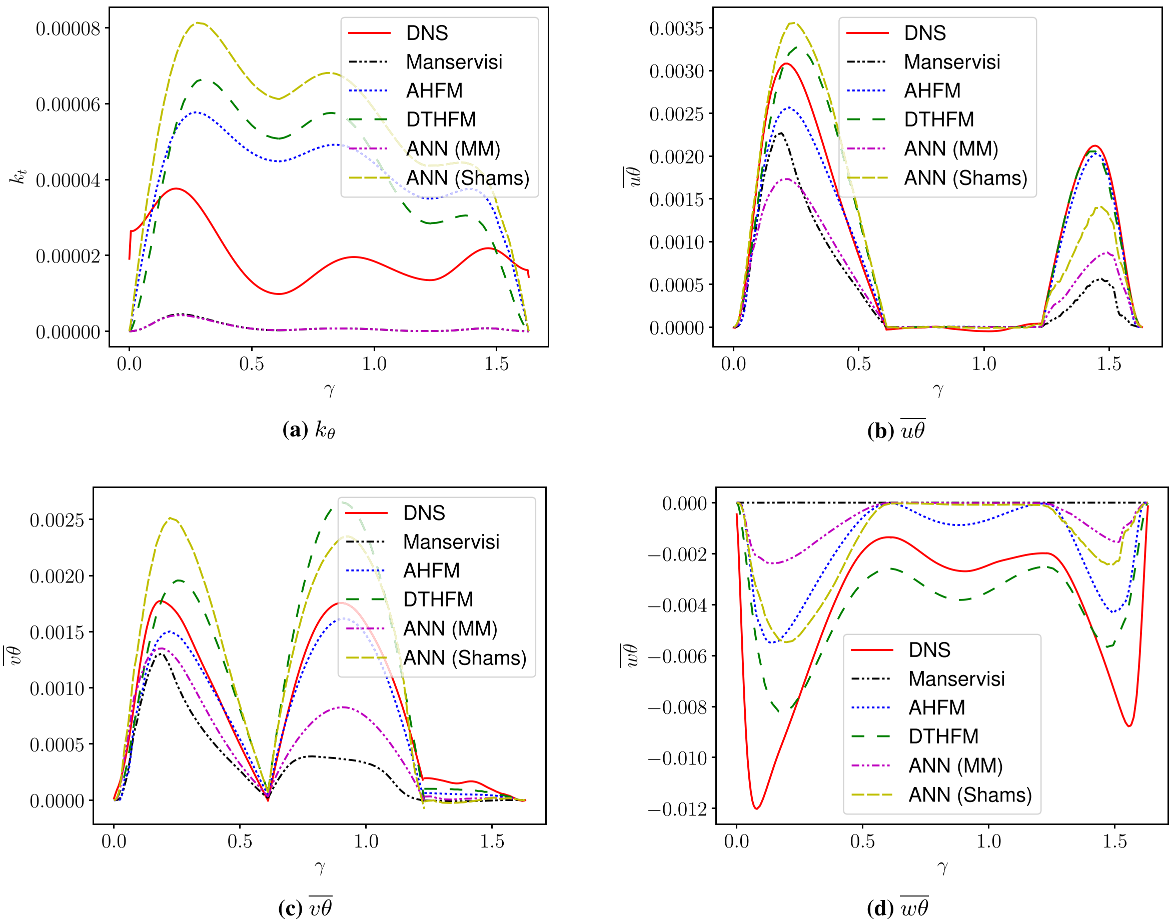

Fig. 20. Comparison of the results achieved with the data-driven model (ANN), the Manservisi model (Manservisi and Menghini, 2014) (MM), the Kays correlation (Kays, 1994), the AHFM (Shams et al., 2019) and the DTHFM (Dehoux et al., 2017) along the border of the flow cell depicted in Fig. 17.

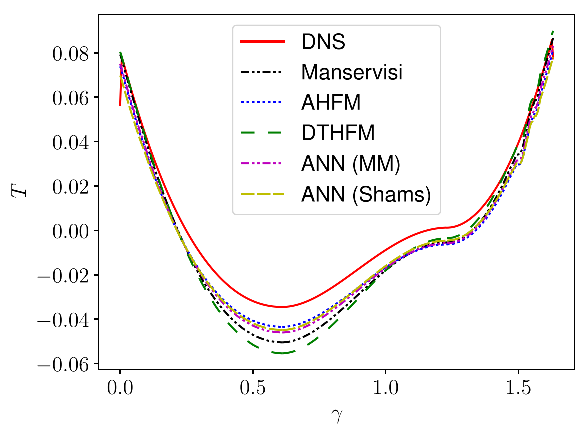

Fig. 21. Temperature obtained with the data-driven model (ANN), the Manservisi model (Manservisi and Menghini, 2014) (MM), the Kays correlation (Kays, 1994), the AHFM (Shams et al., 2019) and the DTHFM (Dehoux et al., 2017) along the border of the flow cell depicted in Fig. 17.

The thermal data-driven model was trained with high-fidelity data and then validated in the OpenFoam environment, where it is coupled with several momentum models (Launder–Sharma $k-\epsilon$, elliptic blending Reynolds stress model) and additional thermal models ($k_\theta-\epsilon_\theta$ model of Manservisi and Meneghini and the k_θ equation of Shams) to compute the turbulent statistics the model needs in input. Due to the specific uncertainties of the combined models, these input quantities can significantly differ from the ones seen by the network during the training. In particular, the Launder–Sharma $k-\epsilon$ model relies on the Boussinesq assumption and does not accurately predict the Reynolds stresses. However, due to the frozen training with DNS data, the predicted dispersion tensor is strongly anisotropic and very sensitive to the Reynolds stress tensor. Hence, the performance of the model significantly decay when a momentum model based on the Boussinesq assumption is coupled with it. Similarly, the sensitivity of the model to the thermal variance and the thermal dissipation rate leads to slightly different heat flux predictions depending on which equations are used to compute these quantities. This lack of robustness limits the application of the data-driven formulation, especially in industrial contexts where eddy-viscosity based momentum turbulence models are generally preferred for their stability and computational cost. Robustness oriented strategies should act on the training database to incorporate modelled data together with their respective uncertainty level, to get a more adaptable data-driven closure.

On the other hand, this limitation highlights that a thermal turbulence model should be developed and applied in combination with its momentum counterpart for a consistent modelling. Based on this evidence, momentum and thermal modelling should advance together to get more accurate heat transfer predictions. The development of new momentum closures could harness even more reference data than for thermal turbulence, which could be efficiently analysed with the same data-driven techniques. Hence, future developments could be aimed at extending the current data-driven approach to the modelling of the Reynolds stresses, thus providing an accurate and complete RANS model for non-isothermal turbulent flows.

Nomenclature

$\mathbf{U}$	[m/s]	Mean velocity
T	[K]	Mean Temperature
$\mathbf{u}$	[m/s]	Velocity fluctuation
θ	[K]	Thermal fluctuation
k	[m^2/s^2]	Turbulent kinetic energy
ϵ	[m^2/s^3]	Turbulent dissipation rate
k_θ	[K^2]	Thermal variance
ϵ_θ	[K^2/s]	Thermal dissipation rate
$\overline{\mathbf{uu}}$	[m^2/s^2]	Reynolds stress
$\overline{\mathbf{u}\theta}$	[m K/s]	Turbulent heat flux
$\mathbf{g}$	[m/s^2]	Gravity vector
ν	[m^2/s]	Molecular viscosity
α	[m^2/s]	Molecular diffusivity
α_T	[m^2/s]	Turbulent diffusivity
δ	[m]	Half channel width
γ	[–]	Blending parameter
$\mathbf{I}$	[–]	Identity tensor

CRediT authorship contribution statement

Matilde Fiore: Conceptualization, Methodology, Software, Investigation, Validation, Writing – original draft, Writing – review & editing. **Lilla Koloszar:** Conceptualization, Methodology, Supervision, Writing – review & editing. **Miguel Alfonso Mendez:** Methodology, Supervision, Writing – review & editing. **Matthieu Duponcheel:** Data curation, Methodology, Supervision, Writing – review & editing. **Yann Bartosiewicz:** Conceptualization, Methodology, Supervision, Writing – review & editing.

Declaration of competing interest

The authors declare the following financial interests/personal relationships which may be considered as potential competing interests: Matilde Fiore reports financial support was provided by FNRS.

Data availability

The data that has been used is confidential.

Acknowledgements

M. Fiore is supported by a F.R.S.-FNRS FRIA, Belgium grant and gratefully acknowledges Prof. Diego Angeli, Prof. Iztok Tiselj and Dr. Jure Oder for providing their datasets, as well as Dr. Clyde Fare from IBM for his valuable suggestions during the course of this work.

References

Abe, K., Kondoh, T., Nagano, Y., 1994. A new turbulence model for predicting fluid flow and heat transfer in separating and reattaching flows—I. Flow field calculations. Int. J. Heat Mass Transfer 37 (1), 139–151.
Abe, K., Kondoh, T., Nagano, Y., 1995. A new turbulence model for predicting fluid flow and heat transfer in separating and reattaching flows—II. Thermal field calculations. Int. J. Heat Mass Transfer 38 (8), 1467–1481.
Angeli, D., Fregni, A., Stalio, E., 2019. Direct numerical simulation of turbulent forced and mixed convection of LBE in a bundle of heated rods with P/D=1.4. Nucl. Eng. Des. 355, 110320.
Arien, B., et al., 2004. Assessment of Computational Fluid Dynamic codes for Heavy Liquid Metals-ASCHLIM. EC-Con. FIKW-CT-2001-80121-Final Report.
Bricteux, L., Duponcheel, M., Winckelmans, G., Tiselj, I., Bartosiewicz, Y., 2012. Direct and large eddy simulation of turbulent heat transfer at very low Prandtl number: Application to lead–bismuth flows. Nucl. Eng. Des. 246, 91–97.
Dehoux, F., Benhamadouche, S., Manceau, R., 2017. An elliptic blending differential flux model for natural, mixed and forced convection. Int. J. Heat Fluid Flow 63, 190–204.
Duponcheel, M., Bricteux, L., Manconi, M., Winckelmans, G., Bartosiewicz, Y., 2014. Assessment of RANS and improved near-wall modeling for forced convection at low Prandtl numbers based on LES up to Reτ=2000. Int. J. Heat Mass Transfer 75, 470–482.
Duraisamy, K., Iaccarino, G., Xiao, H., 2019. Turbulence modeling in the age of data. Annu. Rev. Fluid Mech. 51, 357–377.
Fiore, M., Koloszar, L., Mendez, M.A., Duponcheel, M., Bartosiewicz, Y., 2021. A physics-oriented data-driven approach to thermal turbulence modelling. In: Proc. 15th International Conference on Heat Transfer, Fluid Mechanics and Thermodynamics. Virtual Conference.
Fiore, M., Koloszar, L., Mendez, M.A., Duponcheel, M., Bartosiewicz, Y., 2022. Physics-constrained machine learning for thermal turbulence modelling at low Prandtl numbers. arXiv preprint arXiv:2201.06301.
Geankoplis, C.J., 2003. Transport Processes and Separation Process Principles:(Includes Unit Operations). Prentice Hall Professional Technical Reference.
Grötzbach, G., 2013. Challenges in low-Prandtl number heat transfer simulation and modelling. Nucl. Eng. Des. 264, 41–55.
Jiang, C., Vinuesa, R., Chen, R., Mi, J., Laima, S., Li, H., 2021. An interpretable framework of data-driven turbulence modeling using deep neural networks. Phys. Fluids 33 (5), 055133.
Kawamura, H., Abe, H., Shingai, K., 2000. DNS of turbulence and heat transport in a channel flow with different Reynolds and Prandtl numbers and boundary conditions. Turbul., Heat Mass Transf. 3, 15–32.
Kays, W.M., 1994. Turbulent Prandtl number. Where are we? ASME Trans. J. Heat Transfer 116, 284–295.
Launder, B.E., Sharma, B.I., 1974. Application of the energy-dissipation model of turbulence to the calculation of flow near a spinning disc. Lett. Heat Mass Transf. 1 (2), 131–137.
Lazeroms, W., Brethouwer, G., Wallin, S., Johansson, A., 2013. An explicit algebraic Reynolds-stress and scalar-flux model for stably stratified flows. J. Fluid Mech. 723, 91–125.
Li, Q., Schlatter, P., Brandt, L., Henningson, D.S., 2009. DNS of a spatially developing turbulent boundary layer with passive scalar transport. Int. J. Heat Fluid Flow 30 (5), 916–929.
Ling, J., Jones, R., Templeton, J., 2016a. Machine learning strategies for systems with invariance properties. J. Comput. Phys. 318, 22–35.
Ling, J., Kurzawski, A., Templeton, J., 2016b. Reynolds averaged turbulence modelling using deep neural networks with embedded invariance. J. Fluid Mech. 807, 155–166.
Maddox, W., Garipov, T., Izmailov, P., Vetrov, D., Wilson, A.G., 2019. A simple baseline for bayesian uncertainty in deep learning. arXiv preprint arXiv:1902.02476.
Manceau, R., 2005. An improved version of the elliptic blending model application to non-rotating and rotating channel flows. In: Proc. Fourth International Symposium on Turbulence and Shear Flow Phenomena. Begel House Inc..
Manceau, R., 2015. Recent progress in the development of the Elliptic Blending Reynolds-stress model. Int. J. Heat Fluid Flow 51, 195–220.
Manservisi, S., Menghini, F., 2014. A CFD four parameter heat transfer turbulence model for engineering applications in heavy liquid metals. Int. J. Heat Mass Transfer 69, 312–326.
Maulik, R., Sharma, H., Patel, S., Lusch, B., Jennings, E., 2021. Deploying deep learning in OpenFOAM with TensorFlow. In: Proc. AIAA Scitech 2021 Forum. p. 1485.
Oder, J., Shams, A., Cizelj, L., Tiselj, I., 2019. Direct numerical simulation of low-Prandtl fluid flow over a confined backward facing step. Int. J. Heat Mass Transfer 142, 118436.
Papukchiev, A., Roelofs, F., Shams, A., Lecrivain, G., Ambrosini, W., 2015. Development and application of computational fluid dynamics approaches within the European project THINS for the simulation of next generation nuclear power systems. Nucl. Eng. Des. 290, 13–26.
Roelofs, F., 2018. Thermal Hydraulics Aspects of Liquid Metal Cooled Nuclear Reactors. Woodhead Publishing.
Schmelzer, M., Dwight, R.P., Cinnella, P., 2019. Machine learning of algebraic stress models using deterministic symbolic regression. arXiv preprint arXiv:1905.07510.
Shams, A., 2018. The importance of turbulent heat transfer modelling in low-prandtl fluids. In: Proc. Advances in Thermal Hydraulics (ATH 2018), ANS Winter Meeting Embedded Topical, November, Orlando, FL.
Shams, A., De Santis, A., Roelofs, F., 2019. An overview of the AHFM-NRG formulations for the accurate prediction of turbulent flow and heat transfer in low-Prandtl number flows. Nucl. Eng. Des. 355, 110342.
Shams, A., Roelofs, F., Tiselj, I., Oder, J., Bartosiewicz, Y., Duponcheel, M., Niceno, B., Guo, W., Stalio, E., Angeli, D., et al., 2020. A collaborative effort towards the accurate prediction of turbulent flow and heat transfer in low-Prandtl number fluids. Nucl. Eng. Des. 366, 110750.
Singh, A.P., Duraisamy, K., Zhang, Z.J., 2017. Augmentation of turbulence models using field inversion and machine learning. In: Proc. 55th AIAA Aerospace Sciences Meeting. p. 0993.
So, R., Jin, L., Gatski, T., 2004. An explicit algebraic Reynolds stress and heat flux model for incompressible turbulence: Part I Non-isothermal flow. Theor. Comput. Fluid Dyn. 17 (5–6), 351–376.
So, R., Sommer, T., 1996. An explicit algebraic heat-flux model for the temperature field. Int. J. Heat Mass Transfer 39 (3), 455–465.
Spencer, A., Rivlin, R., 1997. The theory of matrix polynomials and its application to the mechanics of isotropic continua. In: Collected Papers of RS Rivlin. Springer, pp. 1071–1098.

Tarantino, M., Roelofs, F., Shams, A., Batta, A., Moreau, V., Di Piazza, I., Gershenfeld, A., Planquart, P., 2020. SESAME project: advancements in liquid metal thermal hydraulics experiments and simulations. EPJ Nucl. Sci. Technol. 6, 18.

Tiselj, I., Bergant, R., Mavko, B., Bajsic, I., Hetsroni, G., 2001. DNS of turbulent heat transfer in channel flow with heat conduction in the solid wall. J. Heat Transf. 123 (5), 849–857.

Tracey, B.D., Duraisamy, K., Alonso, J.J., 2015. A machine learning strategy to assist turbulence model development. In: Proc. 53rd AIAA Aerospace Sciences Meeting. p. 1287.

Wikström, P., Wallin, S., Johansson, A.V., 2000. Derivation and investigation of a new explicit algebraic model for the passive scalar flux. Phys. Fluids 12 (3), 688–702.

Yin, Y., Yang, P., Zhang, Y., Chen, H., Fu, S., 2020. Feature selection and processing of turbulence modeling based on an artificial neural network. Phys. Fluids 32 (10), 105117.

Zhang, Z.J., Duraisamy, K., 2015. Machine learning methods for data-driven turbulence modeling. In: Proc. 22nd AIAA Computational Fluid Dynamics Conference. p. 2460.